ACS APPLIED MATERIALS & INTERFACES

www.acsami.org

Research Article

Unexpected Penetration of CO Molecule into Zeolitic Micropores Almost Plugged by CuCl via π-Complexation of CO-CuCl

Chan Hyun Lee,*,‡ Kwangsoo Kim,‡ Jisoo Kim, Kanghee Cho, Sang-Sup Han, Hyun Wook Kim, Ki Bong Lee, Byung-Hyun Kim, Jong Hyeok Park, Kyoungsoo Kim, and Jong-Ho Park*

Cite This: *ACS Appl. Mater. Interfaces* 2023, 15, 27411−27421

Read Online

ACCESS | Metrics & More | Article Recommendations | Supporting Information

ABSTRACT: Carbon monoxide (CO) is a key reactant in several Fischer−Tropsch processes, including those used in light olefin and methanol syntheses. However, it is highly toxic and causes serious poisoning of noble metal catalysts. Thus, a solid adsorbent that can selectively capture CO, especially at low concentrations, is required. In this study, zeolite Y-based adsorbents in which Cu(I) ions occupy the supercage cation sites (CuCl/Y) are prepared via solid-state ion exchange. Volumetric adsorption measurements reveal that the Cu(I) ions significantly enhance CO adsorption in the low-pressure range by π-complexation. Furthermore, unexpected molecular sieving behavior, with extremely high CO/CO_2 selectivity, is observed when excess CuCl homogeneously covers the zeolite pore structures. Thus, although CO has a larger kinetic diameter, it can penetrate the zeolite supercage while smaller molecules (i.e., Ar and CO_2) cannot. Density functional theory calculations reveal that CO molecules can remain adsorbed in pseudoblocked pores by CuCl, thanks to the strong interaction of C 2p and Cu 3d states, resulting in the high CO/CO_2 selectivity. One of the prepared adsorbents, CuCl/Y with 50 wt % CuCl, is capable of selectively capturing 3.04 mmol g^{-1} of CO with a CO/CO_2 selectivity of >3370.

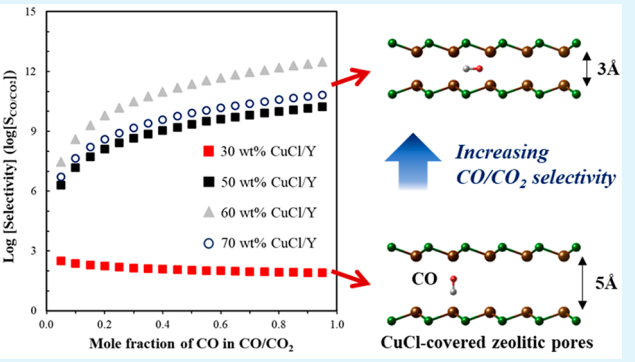

KEYWORDS: *Molecular sieving, π-complexation, adsorbent, kinetic diameter, density functional theory*

INTRODUCTION

Adsorption using solid adsorbents is a key technology in modern chemical engineering processes. Since most chemical reactions generate byproducts, a separation process is essential to selectively produce the desired compounds. Solid adsorbents can selectively capture or remove specific compounds, through a range of different molecular transfer phenomena, and their separation performance can be determined by their characteristics, such as pore structure,[1,2] Lewis basicity,[3−5] and hydrophilicity.[6−8] Of the many impurities that must be removed, carbon monoxide (CO) is a ubiquitous compound produced in various chemical industrial processes. Since CO has a high affinity for transition metals and readily poisons metal catalysts, the concentration of CO should be restricted to a maximum of several parts per million (ppm). For example, CO is a typical byproduct in methane steam reforming or water gas shift reactions for large-scale hydrogen production.[9−11] When powering H_2 fuel cells, the hydrogen used must meet the crucial criteria of having a CO content of less than 0.2 ppm.[12,13]

The CO removal process using solid adsorbents has been the subject of many previous studies, and there are several different types of solid adsorbents that are available for selectively capturing CO in multicomponent gases. Previous reports indicate that activated carbon,[14,15] zeolites,[16,17] and metal−organic frameworks (MOFs)[18,19] have been widely used in CO removal processes. Despite the fact that such adsorbents are designed with unique pore structures that can selectively sieve CO over other components, the separation performance may be significantly reduced at low pressures because the driving force for internal diffusion through the pores is quite low. More importantly, their working capacities for CO decrease as if the other molecules present in a mixed gas stream have similar kinetic diameters. Carbon dioxide (CO_2) is also a typical byproduct in CO chemistry, and the kinetic diameter of CO_2 is known to be 3.30 Å, which is similar to that of CO (3.76 Å).[20] In this context, many previous studies have focused on chemical additives that increase CO affinity.[21−26] Many researchers have reported that ions such as Cu(I) and Ag(I) have the potential to increase the affinity for CO by π-complexation.[27] Such π-complexation bonds are stronger than those formed by van der Waals forces alone, and this is the origin of the higher adsorption

Received: April 5, 2023
Accepted: May 12, 2023
Published: May 26, 2023

capacity and selectivity for CO of these adsorbents. More importantly, complexation bonds are still weak enough to be broken by commonly used operational conditions, such as increasing the temperature or reducing the pressure.[28,29] However, such modified porous materials are thus far limited to selectively capturing only one component from mixtures of molecules with similar sizes.

Here, new solid adsorbents incorporating Cu(I) ions selectively substituted at zeolite Y cation sites are designed and synthesized by solid-state ion exchange using a CuCl additive. The effect of CuCl loading amount on CO and CO_2 adsorption uptake is investigated by systematic characterization including volumetric adsorption measurements and density functional theory calculation. In addition, we report on the unexpected CO diffusion behavior through the pseudoblocked pores by CuCl and the design of novel adsorbents with high CO/CO_2 selectivity using it.

EXPERIMENTAL SECTION

Materials and Synthesis Procedures. Ammonium chloride (NH_4Cl; 98.5%, Samchun Chemicals) and copper chloride (CuCl; ReagentPlus, 99.97%, Sigma-Aldrich) were used in the synthesis procedures without further treatment. Zeolite Y samples were purchased in Na form from UOP (USA) and ground into powder using a mortar. For the synthesis of NH_4^+ ion-exchanged zeolite Y (NH_4Y), the sodium ions in the zeolite Y samples were exchanged with ammonium ions. 15 g of pristine zeolite Y was suspended in 1000 mL of deionized water, dissolved with 53.5 g of NH_4Cl, and stirred for 24 h at room temperature. After that, the precipitate was separated by vacuum filtration, washed with H_2O, and then dried at 120 °C for 24 h. The same procedure was repeated three times to obtain the product zeolite NH_4Y with sufficient ion exchange. Zeolite CuCl/Y adsorbents were prepared by a solid-state ion exchange method. For the synthesis, a predetermined amount of CuCl and NH_4Y zeolite were well mixed and physically ground for 10 min. The CuCl loading amount was varied between 10 and 70 wt %, based on the total weight of the $CuCl/NH_4Y$ physical admixture (3 g). Then, the physical admixture was activated stepwise under vacuum (<1 Pa) conditions. The solid was initially degassed at room temperature until the pressure fell below 1 Pa; then, the temperature was increased stepwise to 80, 150, and then 350 °C and maintained at these temperatures for 1, 3, and 15 h, respectively. The resultant adsorbents were labeled according to the wt % of CuCl in the zeolite CuCl/Y.

Characterization of Prepared Zeolite CuCl/Y Adsorbent. The textual properties of the prepared adsorbents were analyzed using volumetric adsorption measurement. Specifically, the Brunauer–Emmett–Teller (BET) surface area, total pore volume, and micropore volume were measured through the Ar adsorption at −186 °C using a BelSorb Max II (Bel Japan) instrument. Before the analysis, the sample was first degassed using a vacuum pump at room temperature for 2 h until the pressure was below 1 kPa. Then, the reactor was heated to 350 °C and maintained at that temperature to remove impurities for 3 h. The Ar adsorption measurement was conducted after sinking the sample cell into a liquid Ar bath, and the Ar adsorbed amount was calculated at different partial pressures (10^{-5}–1.0 bar). The crystalline phases of the zeolite CuCl/Y adsorbents were measured using an X-ray diffractometer (XRD; D/Max 2200, Rigaku, Japan) with Cu Kα radiation (λ = 0.15418 nm) at 60 kV and 300 mA. The atomic molar fractions were determined by using an energy-dispersive spectroscopy (EDS) unit mounted onto a scanning electron microscope (SEM; S-4800, Hitachi, Japan). The morphology and atomic dispersion mapping images were acquired via transmission electron microscopy (TEM; FEI/TECNAI G2).

The CO and CO_2 adsorption characteristics were measured using volumetric adsorption analyzers (Tristar, Micromeritics and Bel-mini, Bel Japan). The adsorption uptakes were measured by calculating the cumulative dosing amount at partial pressures between 10^{-5} and 1 bar. The measured CO and CO_2 adsorption isotherms for the zeolite CuCl/Y samples at 25 °C were fitted with proper models in order to investigate their adsorption characteristics in detail. A single Langmuir isotherm model (eq 1) and dual-site Langmuir–Freundlich model (eq 2) were used for simulating the CO_2 and CO isotherms, respectively.

$$Q_{CO_2} = \frac{Q_{max} b(P/P_0)}{1 + b(P/P_0)} \quad (1)$$

$$Q_{CO} = \frac{Q_{max,1} b_1 (P/P_0)^{n_1}}{1 + b_1 (P/P_0)^{n_1}} + \frac{Q_{max,2} b_2 (P/P_0)^{n_2}}{1 + b_2 (P/P_0)^{n_2}} \quad (2)$$

where Q_{max} indicates the theoretical adsorption capacity (mmol g^{-1}) for a certain adsorption site, b is the pressure parameter, and n is the Freundlich parameter.

In situ diffuse reflectance infrared Fourier-transform spectroscopy (DRIFTS) spectra were collected on a Nicolet 10 (Thermo Fisher Scientific) spectrometer equipped with a PRAYING MANTIS sample collector at a spectral resolution of 4 cm^{-1} and using 64 accumulated scans. The collected spectra were converted into Kubelka–Munk (MK) units. CO adsorption using DRIFTS analysis was implemented with different CO partial pressures. The measurements were organized consecutively, first increasing the concentration of CO to 20% and subsequently to 50%, 80%, and then 100% by maintaining the adsorption temperature to 30 °C. CO-TPD measurements were performed by using an AutoChem II instrument (Micrometrics, USA). For the analysis, about 50 mg of each sample was loaded in a quartz tube reactor and pretreated at 350 °C under He flows for 2 h. After this thermal treatment, the temperature was cooled to 50 °C and then exposed to a 1% CO flow (balanced with He) for 2 h. The thermal conductivity detector (TCD) signal was monitored as the temperature was raised to 500 °C with a ramping rate of 10 °C min^{-1}.

Computational Methods. All theoretical investigations were conducted by performing spin-polarized DFT calculations using the Vienna ab initio simulation package (VASP)[30−33] based on the projector augmented wave (PAW) pseudopotentials.[34,35] The $3d^{10}4s^1$, $3s^23p^5$, $2s^22p^2$, $2p^42s^2$, and $3s^23p^6$ valence electrons of Cu, Cl, C, O, and Ar, respectively, were treated explicitly as valence states in the Kohn–Sham equations. The Perdew–Burke–Ernzerhof (PBE) exchange–correlation functional with a generalized gradient approximation (GGA)[36] form was employed. To accurately describe interactions between a molecule and substrate, long-range dispersion forces, as suggested by Grimme et al.,[37] were also taken into account in all the calculations. While the overall adsorption, when corrected for vdW, was marginally stronger than that without the correction, the molecular adsorption behavior remained consistent regardless of whether the vdW correction was applied or not (Figure S1).

A kinetic energy cutoff of 600 eV for the Kohn–Sham single-electron wave functions was adopted. The convergence criteria for total electronic energy and geometry optimizations were set to 10^{-5} eV and 0.02 eV $Å^{-1}$, respectively. The Brillouin zone was sampled using the Monkhorst–Pack scheme with 2 × 2 × 1 k-points.[38]

The adsorption energy (E_{ads}) was calculated from the following eq 3:

$$E_{ads} = E_{tot}(\text{molecule} + \text{substrate}) - \{E_{tot}(\text{substrate}) + E_{tot}(\text{molecule})\} \quad (3)$$

where E_{tot}(molecule + substrate) indicates the total energy of a single molecule adsorbed on the substrate and E_{tot}(substrate) and E_{tot}(molecule) represent the total energy of the bare substrate and the single molecule in a vacuum. The surface orientation of CuCl was set to (111) as the CuCl(111) surface was found to be the most stable in terms of surface free energy. A vacuum region of 20 Å was added to the slab model system to minimize the image–image interactions due to the periodic boundary conditions. During geometry optimization, the adsorbed molecules were allowed to fully relax while the substrate was fixed at its bulk geometry. Including a Hubbard U term as proposed by Dudarev et al.[39] for the Cu d electrons produced a negligible effect on the CO and CO_2 adsorption energy calculations, and hence, we were able to retain the conclusion drawn from the conventional DFT calculations.

https://doi.org/10.1021/acsami.3c04849
ACS Appl. Mater. Interfaces 2023, 15, 27411−27421

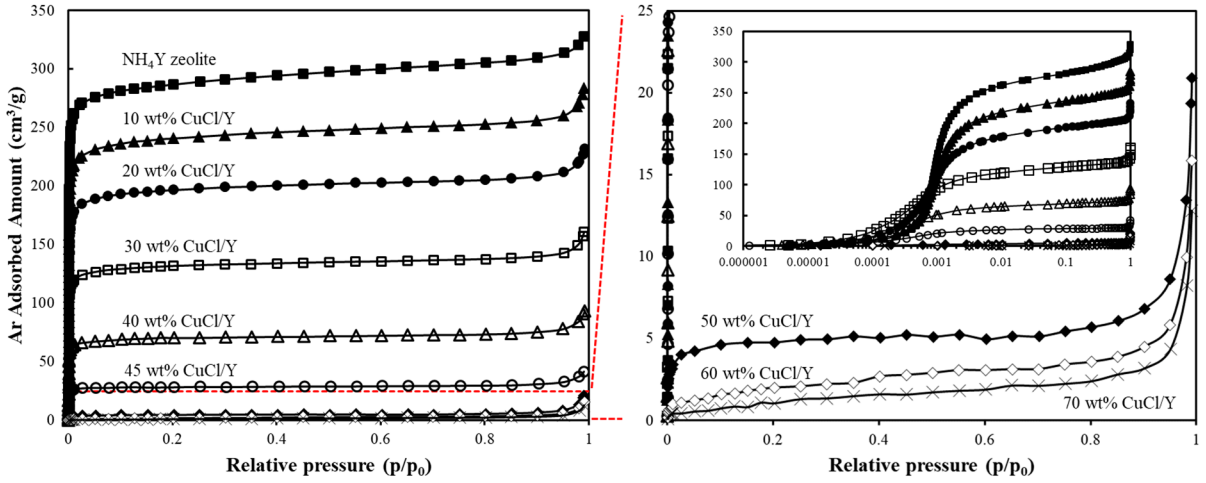

Figure 1. Ar adsorption isotherms at −186 °C for NH_4Y and zeolite CuCl/Y adsorbents with various amounts of CuCl in the range of 0−70 wt %. Inset, right: isotherms plotted versus relative pressure on a logarithm scale.

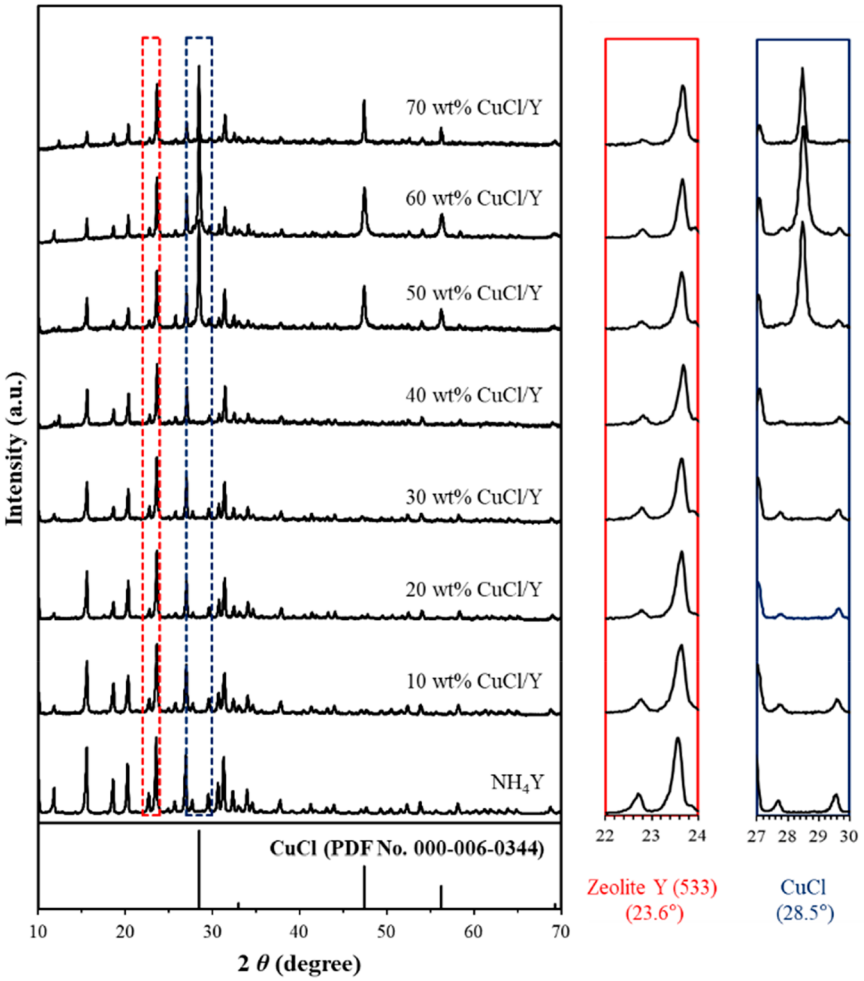

Figure 2. X-ray diffraction spectra of zeolite CuCl/Y adsorbents prepared using different CuCl loading amounts (0−70 wt %). Red and blue dotted area represents a series of enlarged patterns for zeolite Y (533) plane (2θ = 23.6°) and CuCl (2θ = 28.5°), respectively.

RESULTS AND DISCUSSION

Textural Properties of Ion-Exchanged Zeolite Y. As shown in Figure 1, the Ar adsorption isotherms for zeolite Y vary as their cation sites are occupied by different ions. NH_4Y has a very steep slope in the lower pressure range (P/P_0 < 0.05), and the BET surface area is measured as 810 $m^2\ g^{-1}$. This indicates that the NH_4^+ ions are uniformly dispersed in the cationic sites in the zeolite cage structure and do not impede diffusion through the pores. Upon increasing the CuCl loading, the measured Ar adsorbed amount gradually decreases but the adsorption characteristics of the narrow micropore volumes can still be

https://doi.org/10.1021/acsami.3c04849
ACS Appl. Mater. Interfaces 2023, 15, 27411−27421

observed when the loading is 40 wt % or less. When the amount of CuCl is 50 wt % or more, the Ar adsorption isotherms become almost flat because the excess CuCl present on the sorbent surface blocks the pore structure, preventing the Ar adsorbate from penetrating into the pores. Specifically, the pore structure of 50 wt % CuCl/Y seems to be mostly blocked by CuCl, but a very small amount of narrow micropore structures remain. Furthermore, the 60 and 70 wt % CuCl/Y adsorbents have very low BET surface areas (<10 m^2 g^{-1}), with all the micropores being blocked by CuCl. During solid-state ion exchange, the Cu(I) ions in the CuCl additive migrate so as to occupy cationic sites in the zeolite Y framework of NH_4Y, liberating NH_4^+ ions, which react with residual chlorines to form the NH_4Cl salt. The NH_4Cl byproduct can be easily sublimated at temperatures above 250 °C.[40] The theoretical maximum achievable loading amount for Cu(I) ions occurs when approximately stoichiometric NH_4-form of zeolite Y is mixed with 24.6 wt % CuCl, as shown in eq 4.

$$(NH_4)_{56}[Al_{56}Si_{136}O_{384}]{:}250H_2O + 56CuCl \leftrightarrow (Cu)_{56}[Al_{56}Si_{136}O_{384}]{:}250H_2O + 56NH_4Cl \quad (4)$$

The crystalline structural changes for zeolite CuCl/Y adsorbents can be found in the XRD patterns in Figure 2. All samples exhibit strong peaks located at 11.9°, 15.6°, 18.7°, 20.4°, 23.6°, 26.9°, and 31.4°, and these peaks can be assigned to diffractions from the (311), (331), (511), (440), (533), (642), and (555) planes, respectively.[41] For CuCl doped samples (except NH_4Y), the main XRD peaks due to cations in the zeolite framework, namely, the (311), (331), and (511) diffraction peaks, decrease in intensity as the amount of CuCl loading increases. From this, it can be inferred that the cation sites occupied by NH_4^+ ions are successfully replaced by Cu(I) ions through solid-state ion exchange. Moreover, additional CuCl peaks are observed for the adsorbents with CuCl loadings of 40 wt % or more. This means that excess CuCl is present on the surface of the adsorbent after the Cu(I) ions have all been replaced by solid-state ion exchange. The amount of crystalline CuCl on the adsorbents can be calculated from the ratio of XRD peak intensities for CuCl (28.5°) and zeolite Y (23.6°), and the results are plotted in Figure S2. It is apparent from these results that a relatively small amount of the crystalline phase of CuCl exists in 40 wt % CuCl/Y, and the amount of the CuCl crystalline phase gradually increases up to loading amounts of 60 wt %. A similar trend can also be seen in the SEM-EDS analysis (Table 1). In order to observe the localization of the excess CuCl on zeolite Y framework, TEM analysis is also applied to characterize the highly CuCl loaded zeolite Y adsorbents. As shown in Figure 3a–c, the TEM images of the adsorbents with

Table 1. Measured Atomic Molar Ratios for Zeolite CuCl/Y Adsorbents from SEM-EDS Analysis

	elements (mol %)				
sample	Na	Al	Si	Cl	Cu
0 wt % CuCl/Y[c]	3.84	26.01	70.15	n.d.[b]	n.d.[b]
10 wt % CuCl/Y	4.93[a]	23.33	62.49	n.d.[b]	9.25[a]
20 wt % CuCl/Y	n.d.[b]	21.61	60.30	2.26	15.83
30 wt % CuCl/Y	n.d.[b]	18.50	51.66	8.79	21.05
40 wt % CuCl/Y	n.d.[b]	13.09	35.77	20.85	30.29
50 wt % CuCl/Y	n.d.[b]	10.72	29.84	25.84	33.59
60 wt % CuCl/Y	n.d.[b]	10.30	28.39	25.58	35.72
70 wt % CuCl/Y	n.d.[b]	11.52	30.26	27.80	30.41

[a]Peaks overlapped for NaKα (1.041 keV) and CuLα (0.928 keV). [b]Not detected. [c]Same as NH_4Y.

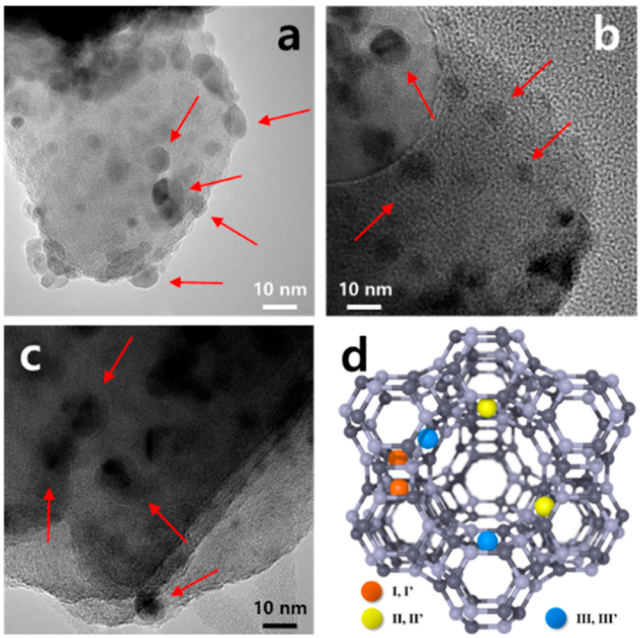

Figure 3. TEM images of zeolite CuCl/Y with (a) 50, (b) 60, and (c) 70 wt % CuCl. (d) Schematic zeolite Y framework with possible cationic sites indexed as I, I′, II, II′, III, and III′.

CuCl loadings of ≥50 wt % depict particles of 2 to 10 nm size on the adsorbent surface, and the particle size is independent of the loading amount. For zeolite Y, the cation sites are located in sodalite cages and hexagonal prisms to balance the negative charge of the FAU framework (Figure 3d).[42,43] The Cu(I) ions at cation sites II and III can coordinate with Cl^- ions to form Cu_3Cl^{2+} complexes close to the 12-ring cages, and the other ions at the I and I′ sites can form a $Cu_{16}Cl_7^{21+}$ complex in a FAU supercage.[44] Thus, the excess CuCl occupies the pore structures of zeolite Y, rendering its microporosity poor and hindering Ar diffusion during the adsorption measurement at −186 °C (87 K). The elemental mapping images for the zeolite CuCl/Y samples with 50, 60, and 70 wt % CuCl/Y in Figure S3 show that not only Cu but also the Cl atoms are dispersed on the surface of zeolite, and CuCl particles are aggregated in some spots (see red arrows in Figure 3a–c). These results support the conclusion that excess CuCl occupies the pores in the zeolite Y structure resulted in reduced the BET specific surface area and total pore volume.

CO_2 and CO Adsorption Properties of Zeolite CuCl/Y.

Single-gas adsorption uptake data for CO and CO_2, as a function of the amount of CuCl in the zeolite adsorbent, are shown in Figure 4a–c. Considering that the pore structures are gradually blocked as the amount of CuCl increases, different trends of zeolite CuCl/Y for CO and CO_2 adsorption seem quite interesting. The CO_2 uptake is measured as 4.85 mmol g^{-1} for NH_4Y, and it significantly decreases to below 0.3 mmol g^{-1} for zeolite CuCl/Y with 50, 60, and 70 wt % CuCl. As shown in Figure 4a, the measured CO_2 adsorption behavior of the different zeolite CuCl/Y samples have a typical Langmuir isotherm. In contrast, the CO adsorption trend is completely different from that of CO_2. The measured CO adsorption uptake

https://doi.org/10.1021/acsami.3c04849
ACS Appl. Mater. Interfaces 2023, 15, 27411−27421

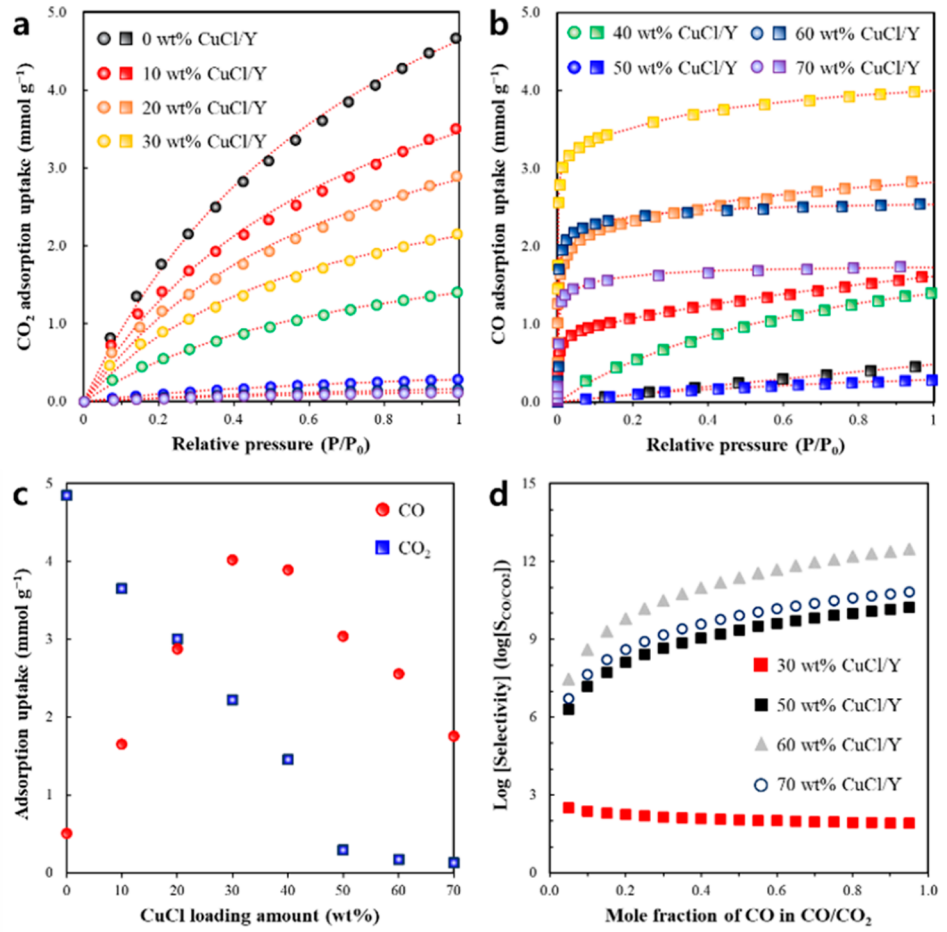

Figure 4. (a) CO_2 and (b) CO adsorption isotherms for zeolite CuCl/Y adsorbents with *x* wt % CuCl as a function of relative pressure (symbols) with fits obtained using a Langmuir model (red dotted line). (c) CO and CO_2 adsorption uptakes for CuCl/Y adsorbents at 25 °C and 1 bar. (d) IAST CO/CO_2 selectivity for CuCl/Y with 30, 50, 60, and 70 wt % CuCl loadings as a function of CO partial pressure at 25 °C.

versus CuCl amount has a volcano shape, with a peak at a CuCl loading of 30 wt %. The CuCl/Y adsorbents have significantly higher adsorption capacities than pristine NH_4Y (i.e., 0 wt % CuCl/Y). The CO adsorption uptake in that case is measured as 0.51 mmol g^{-1}, and the value increases to 4.03 mmol g^{-1} for its 30 wt % CuCl counterpart. The calculated CO adsorption performance is similar or slightly higher compared to those of previous reported CuCl-loaded zeolite adsorbents (2.78−3.79 mmol g^{-1}).[25,45,46] The outstanding CO adsorption uptake gradually decreases as the loading amount increases beyond 30 wt %, which is due to the decreased pore volume with the CuCl overloading. Figure 4b shows the measured CO isotherms for zeolite CuCl/Y with different CuCl loadings. Once CuCl is incorporated within zeolite Y, the affinity for CO at low pressures (P/P_0 < 0.05) can be significantly enhanced by π-complexation, as has already been reported in many previous studies.[47−49] Moreover, the CO adsorption isotherms could be fitted using a dual-site Langmuir−Freundlich isotherm model, which considers two consecutive adsorption steps: (1) adsorption by micropores and (2) multilayer adsorption by π-complexation. As shown in Table S1, the Langmuir−Freundlich parameters from CO isotherms have some interesting trends unlike the case of CO_2. Capillary condensation through the micropores, the adsorption behavior corresponding to the first term in the isotherm model, is not easily observed as more CuCl is mixed with NH_4Y, but the adsorption behavior due to π-complexation (the second term in the isotherm model) can be observed even at high CuCl loading amounts. In particular, CO adsorption uptake does not decrease as rapidly as in the case of CO_2, with relatively high CO adsorption uptakes measured even when the CuCl loading amount is >50 wt %.

Note that the kinetic diameter of CO (3.76 Å) is slightly larger than that of CO_2 (3.30 Å), and because the prepared adsorbents have very low BET surface areas, this behavior is unexpected. In order to examine whether the excellent CO adsorption performance is due to the excess CuCl on the adsorbent surface or not, the CO adsorption uptake of carbon-deposited zeolite Y (zeolite c-Y) loaded with 20 wt % CuCl is measured at 25 °C (detailed synthesis procedures for the zeolite c-Y sample are described in the Supporting Information). As shown in Figure S4, the zeolite CuCl/c-Y sample with 20 wt % CuCl has a very low BET surface area of 3 m^2 g^{-1} and can only adsorb 3.0 μmol g^{-1} of CO. It means that such high adsorption capacity of CO on zeolite CuCl/Y with 50 wt % or more cannot be obtained with the CuCl existing outside of the zeolitic pore structures. This result suggests that the unusual CO adsorption characteristics for the CuCl/Y adsorbents would be caused by factors as yet unknown. This unusual phenomenon makes the zeolite Y that is highly loaded with CuCl exhibit very high CO/CO_2 selectivity (s_{CO/CO_2}), even at very low CO partial pressures. In particular, the CuCl/Y loaded with 30 wt % CuCl can capture a massive amount of gas molecules, not only CO but also CO_2, because

https://doi.org/10.1021/acsami.3c04849
ACS Appl. Mater. Interfaces 2023, 15, 27411−27421

pore structures that capture CO_2 are presented and the cation sites are replaced with Cu(I) ions, which makes bonding with CO via π-complexation favorable. The sample of CuCl/Y with 50 wt % CuCl, in which most of the pores are blocked (S_{BET} = 15 $m^2\ g^{-1}$), has lost almost all of its CO_2 adsorption capacity, but it still demonstrates a very steep CO isotherm at low pressure (<0.1 bar), followed by a slow increase as the pressure increases beyond this point. The adsorption selectivity (s_{CO/CO_2}) can be estimated via the ideal adsorbed solution theory (IAST) approaches as in the following eq 5:

$$s_{CO/CO_2} = \frac{Q_{CO}}{Q_{CO_2}} \Big/ \frac{y_{CO}}{y_{CO_2}} \tag{5}$$

where Q_i indicates the adsorption uptake of the i component (i = CO or CO_2) and y_i is the mole fraction in the gas phase. The calculated IAST model parameters are summarized in Table S2. As shown in Figure 4d, the selectivity for three samples (zeolite CuCl/Y with 50, 60, and 70 wt % CuCl) is found to be $>10^6$ at low pressure (partial pressure <0.1) and then gradually increases as the partial pressure increases, contrary to the zeolite CuCl/Y with 30 wt % CuCl, in which the selectivity decreases with the increase of the CO partial pressure. The present study is unique thus far, however, in finding that highly CuCl loaded samples (50, 60, and 70 wt % CuCl/Y), in which the pores are almost entirely blocked by excess CuCl, still maintain their promising CO adsorption characteristics at low pressures.

Abnormal CO Adsorption Characteristics for Highly CuCl Loaded Zeolite Y. In order to compare the interaction between CO adsorbate and adsorbent, CO-temperature-programmed desorption (CO-TPD) is performed with CO-captured CuCl/Y with 30, 50, and 70 wt % CuCl. As shown in Figure 5a, all samples have similar desorption trends, with a strong desorption peak at a lower temperature (90−120 °C) and broad and weak desorption peak above 150 °C. The first peak, at lower temperature, indicates that the bond between CO and the Cu(I) ions is cleaved, and the second peak, observed at higher temperature, indicates the desorption of CO molecules trapped inside the pores. It is very interesting that the first peak for CuCl/Y with 30 wt % CuCl is quite broad, and its maximum occurs at around 120 °C, while a very intense peak occurs at 97 °C for the zeolites CuCl/Y with 50 and 70 wt % CuCl. Thus, it can be understood that the bond between CO and CuCl additive is modified when excess CuCl homogeneously covers the pores.

The CO species adsorbed on zeolite CuCl/Y with 70 wt % CuCl are identified by DRIFTS, and the result is shown in Figure 5b. Dosing of CO under different partial pressures into the IR cell led to the development of two IR feature characteristics at 2178 and 2151 cm^{-1}, which are widely reported as symmetric and asymmetric vibration bands of CO.[50−52] At the initial adsorption experiment under partial pressure of 0.2 bar, the adsorbed CO is stabilized by the formation of the Cu^+−CO complex as evidenced by C−O vibration at 2108 cm^{-1},[53] while for the CO adsorption at higher CO pressures, the new bands at 2126 and 2017 cm^{-1} appear and their intensities increase rapidly with CO pressure. The peak at 2126 cm^{-1} can be ascribed to the stretching frequency of CO adsorbed on Cu^+ cation with one vacancy.[54] In addition, the band at 2017 cm^{-1} is thought to be a red-shifted form of the peak at 2108 cm^{-1}, which corresponds to stabilized CO on the Cu surface. The lower frequency band indicates an enhancement in the electron density of the hybrid d + s valence bands of these Cu particles, and this can be explained by considering the nature of CO bonding with transition metals

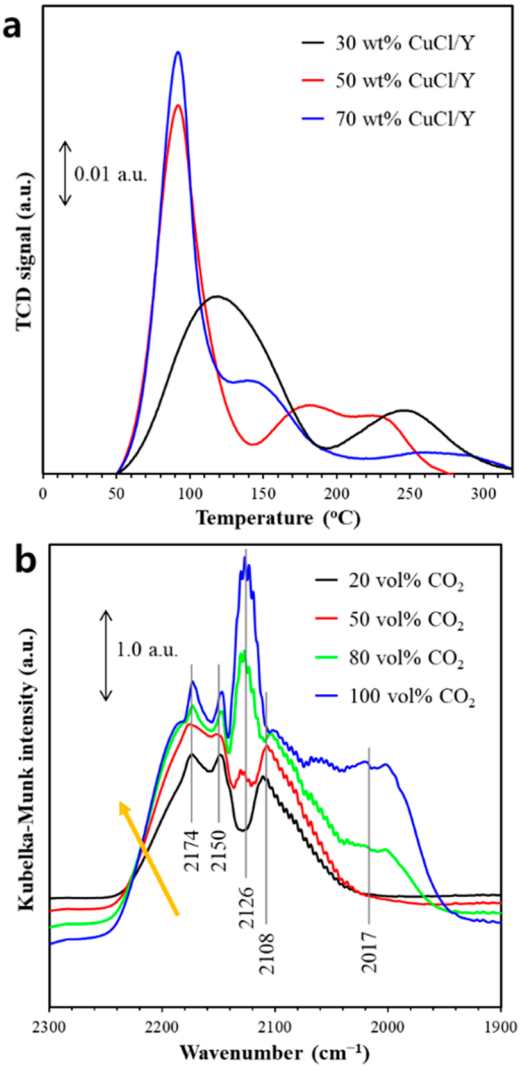

Figure 5. (a) CO-TPD profiles for zeolite CuCl/Y adsorbents with 30, 50, and 70 wt % CuCl. (b) In situ analysis results for zeolite CuCl/Y with 70 wt % CuCl under different CO partial pressures (20, 50, 80, and 100 vol % of CO mixed with N_2).

in terms of a $\sigma-\pi$ bonding model.[55] From these results, we can conclude the CO adsorption mechanism of highly CuCl loaded zeolite Y: (1) two of the packed CO molecules interact with Cu(I) ions near the pore mouth and diffuse through the narrow micropore; (2) trapped CO molecules are stabilized inside the pore by the π-complexation.

Origin of Enhanced CO/CO_2 Selectivity of Highly CuCl Loaded Zeolite Y. DFT calculations are performed to determine the origin of the abnormal CO adsorption characteristics for highly CuCl loaded zeolite Y adsorbents. First, utilizing the quantum mechanical diameter calculations proposed by Mehio et al.,[56] we check whether kinetic diameter changes for the CO and CO_2 molecules upon their adsorptions on the CuCl surface are the main factor behind the enhanced CO/CO_2 selectivity. It is found that the kinetic diameter of a CO molecule when it is adsorbed on a CuCl surface increases from 3.76 to 4.12 Å, as a result of the electron accumulation at the boundary between the C atom of the CO molecule and the Cu atom. In contrast, the change in the kinetic diameter of a CO_2 molecule after adsorption is found to be negligible (3.64 Å) (Figure 6). Therefore, our theoretical investigation into the kinetic diameter

https://doi.org/10.1021/acsami.3c04849
ACS Appl. Mater. Interfaces 2023, 15, 27411−27421

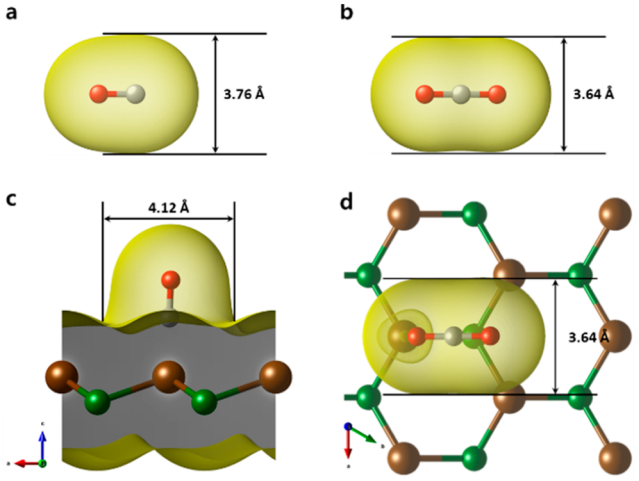

Figure 6. Calculated kinetic diameters of (a, c) CO and (b, d) CO_2 (a, b) before and (c, d) after adsorption on the CuCl surface. Green, brown, gray, and red spheres indicate chlorine, copper, carbon, and oxygen atoms, respectively. The yellow and black colors refer to the boundary and cross-section, respectively, occupied by the electron density with an isosurface level of 0.00093 e $bohr^{-3}$.

changes revealed that the concept of kinetic diameter is insufficient to explain the experimental observation of excellent CO adsorption performance for the excess CuCl loaded zeolite Y samples; the kinetic diameter of a CO molecule increases when the CO molecule interacts with Cu in the CuCl adsorbent surface, which should impede CO adsorption in the pores.

Thus, we next decide to investigate the adsorption behavior of CO and CO_2 molecules on the CuCl surface as a function of pore size. The Cu exposed CuCl(111) surface was selected for our DFT model structures due to its known stability as the most stable orientation, and its peak is the most dominant in the XRD analyses from previous studies;[57,58] the three-coordinate unsaturated Cu(I) site is known as the active center for catalysts.[59] Two CuCl(111) single layers with different interlayer distances are utilized as model structures for the CuCl-loaded zeolite Y samples with different pore sizes. In preliminary simulations, it was found that the adsorption of either a CO or a CO_2 molecule on the CuCl surface takes place at the outer surface of the CuCl layers and that the thickness (number of CuCl layers) dependence of the adsorption energy is found to be negligible; the calculated adsorption energy of a CO molecule on a single layer of CuCl, a bilayer of CuCl, and five layers of CuCl was −1.01, − 0.99, and −1.01 eV, respectively (Table 2). Thus, the zeolite Y structure and the bulk CuCl region are omitted in the simulation for the sake of simplicity. It is found that the CO adsorption (−1.01 eV) is much stronger than the CO_2 adsorption (−0.22 eV) on the CuCl(111) surface. The CO molecule is preferentially adsorbed with the C−O bond perpendicular to the CuCl surface, with a short distance between the CO molecule and Cu atom of 1.84 Å (Figure 7a). In contrast, the optimized structure of a CO_2 molecule interacting with the CuCl layer lies with the C−O bonds in a plane parallel to the surface, and the distance between the surface and CO_2 molecule is also greater (2.47 Å) (Figure 7c). Furthermore, the differential charge density analysis results show that a considerable amount of charge transfer occurs between the adsorbed CO molecule and the CuCl substrate (Figure 7a), while the amount of charge transfer from the adsorbed CO_2 to CuCl was found to be almost negligible (Figure 7c). The C 2p and Cu 3d projected densities of states also reveal that CO adsorption on the CuCl layer results in a strong interaction between the C 2p and Cu 3d states (Figure 7b). However, a slight change in the electronic structure of the Cu 3d states upon CO_2 adsorption was found, as shown in Figure 7d. Both differential charge density and projected density of states analyses indicate that the stronger adsorption of CO than CO_2 on the CuCl surface can be attributed to the interaction between C 2p and Cu 3d states, which results in π-complexation.

Table 2. Energies of CO and CO_2 Adsorption on a CuCl Surface as a Function of CuCl Layer Thickness (Number of Layers)

	adsorption energy (eV)	
number of layers	CO/CuCl	CO_2/CuCl
1	−1.01	−0.22
2	−0.99	−0.24
5	−1.01	−0.27

The effect of pore size is simulated by adjusting the distance between the two CuCl layers, which is defined as the shortest distance between any two Cu ions in different slabs (Figure 8 inset). Figure 8 shows the calculated adsorption energies of a CO and CO_2 molecule on the CuCl layers, as a function of interlayer distance; positive adsorption energies correspond to the adsorption being unfavorable. When the interlayer distance decreases, corresponding to a decrease in pore size, the adsorption energies for both the CO and CO_2 molecules increase. However, the CO adsorption is found to be strong and favorable down to an interlayer distance of approximately 2.5 Å, whereas the CO_2 adsorption becomes energetically unfavorable when the interlayer distance drops to less than 5 Å. Interestingly, the local atomic geometry of a CO molecule adsorbed on the CuCl surface changes from being perpendicular to the CuCl surface to being parallel to it, without a significant increase in adsorption energy, as the interlayer distance is reduced, which allows the CO molecule to remain adsorbed at a wide range of interlayer distances (see also Table 3 and Figure S5). Furthermore, Ar adsorption on the CuCl layers with different interlayer distances is also calculated. Calculations of the adsorption energy of an Ar atom on the CuCl surface as a function of interlayer distance show that Ar adsorption is unfavorable for the interlayer distance <5 Å. This indicates that such pores cannot be detected via Ar adsorption, consistent with the low BET values derived from Ar adsorption isotherms at high CuCl loading. Consequently, the diffusion of CO molecules through narrow micropores of highly CuCl loaded zeolite Y can be successfully explained by the strong interaction of the CO C 2p and 3 d states of Cu in the CuCl surface. It enables favorable CO adsorption with smaller pores, under which conditions the interaction of CO_2 with the CuCl surface is weak or energetically unfavorable. These results are in good agreement with the previous IR study, and ultimately, the absorbed CO molecules are stabilized inside the pore by the π-complexation. Moreover, the DFT calculation also examines the origin of extremely high CO/CO_2 selectivity for highly CuCl loaded zeolite Y adsorbents. This unconventional adsorption property based on diffusion through the "pseudoblocked" narrow micropores is expected to be applied to the design of novel solid sorbents for selective CO removal.

https://doi.org/10.1021/acsami.3c04849
ACS Appl. Mater. Interfaces 2023, 15, 27411−27421

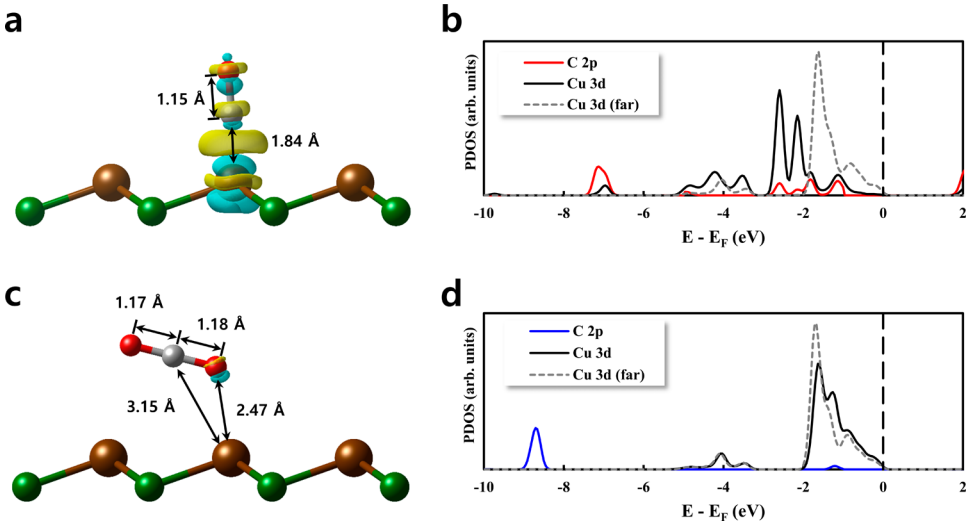

Figure 7. Geometry-optimized atomic structure and its differential charge density of (a) CO and (c) CO_2 on the CuCl surface with an isosurface level of 0.0035 e $bohr^{-3}$. The color coding of atoms is the same as that used in Figure 6. Yellow and cyan colors in the isosurface indicate charge accumulation and depletion, respectively. Projected density of states (PDOS) plots for (b) CO and (d) CO_2 adsorption on the CuCl surface. C 2p states of CO and CO_2 are drawn as red and blue lines, while 3d states of Cu that interact with the given molecule and of Cu far from the given molecule are drawn as solid black and dashed gray lines, respectively.

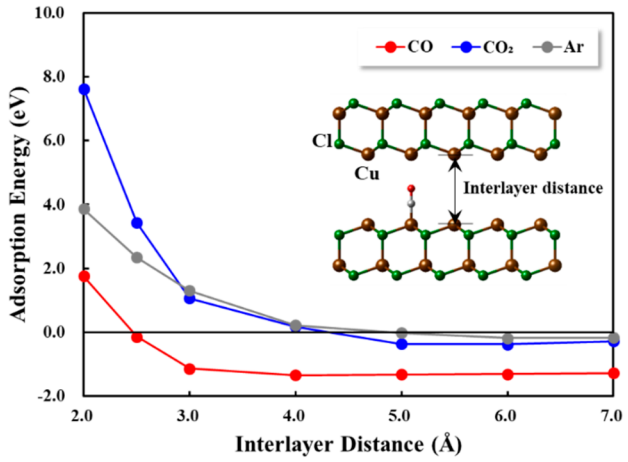

Figure 8. Calculated adsorption energies of CO (red), CO_2 (blue), and Ar (gray) on the CuCl surface as a function of interlayer distance between two CuCl layers (inset).

Table 3. Optimized Geometry of CO and CO_2 Molecules on the CuCl Surface as a Function of Interlayer Distance[a]

	adsorption direction		C−Cu distance (Å)	
interlayer distance (Å)	CO	CO_2	CO	CO_2
2.0	parallel	parallel	1.74	1.84
2.5	parallel	parallel	1.80	1.99
3.0	parallel	parallel	1.87	2.26
4.0	parallel	parallel	2.11	2.77
5.0	perpendicular	parallel	1.81	3.01
6.0	perpendicular	parallel	1.84	3.50
7.0	perpendicular	parallel	1.84	3.56

[a]Corresponding images are shown in Figure S5.

CONCLUSION

In summary, a series of CuCl loaded zeolite Y adsorbents have been successfully synthesized by solid-state ion exchange. As the CuCl loading increases, Cu(I) ions substitute for NH_4^+ cations of the zeolite Y framework before excess CuCl homogeneously covers the adsorbent surface. The prepared zeolite CuCl/Y adsorbent shows completely different adsorption behavior for CO_2 and CO as the CuCl loading amount varies. The adsorption uptakes for CO_2 are rapidly decreased as the micropore structure is blocked by excessive CuCl, whereas it is unexpected that the adsorption behavior of CO is found due to diffusion through the pseudoblocked micropores. In addition, the CuCl incorporated samples interact with CO via relatively strong π-back bonding, even at very low pressures. Systematic characterizations including DRIFTS and DFT computations reveal that the unusual CO adsorption behavior of highly CuCl loaded zeolite Y originates from the strong interaction of C 2p and Cu 3d states via π-complexation. Moreover, the CO molecules can successfully penetrate through pores pseudoblocked by CuCl, thanks to the strong interaction, but other molecules such as Ar and CO_2 are blocked by the CuCl additive. Based on the abnormal CO adsorption characteristics, adsorbents containing pseudoblocked pores exhibit extremely high CO/CO_2 selectivity of over 10^6. The unusual molecular sieving behavior for highly CuCl loaded zeolite Y means that the sorbent has a much higher CO/CO_2 selectivity and adsorption uptake. These results may inspire the future development of CO/CO_2 separation processes and a selective CO removal or trapping system.

ASSOCIATED CONTENT

Supporting Information

The Supporting Information is available free of charge at https://pubs.acs.org/doi/10.1021/acsami.3c04849.

Experimental details for carbon deposited zeolite Y; tables containing isotherm parameters and DFT simulation results; supplementary figures: XRD, TEM, single gas isotherms, and geometry-optimized atomic structures (PDF)

https://doi.org/10.1021/acsami.3c04849
ACS Appl. Mater. Interfaces 2023, 15, 27411−27421

AUTHOR INFORMATION

Corresponding Authors

Jong-Ho Park − *Clean Fuel Laboratory, Korea Institute of Energy Research, Daejeon 34129, Republic of Korea*; Email: jongho@kier.re.kr

Chan Hyun Lee − *Clean Fuel Laboratory, Korea Institute of Energy Research, Daejeon 34129, Republic of Korea; School of Chemical Engineering, University of Ulsan, Ulsan 44610, Republic of Korea*; orcid.org/0000-0002-3529-1018; Email: chhylee@ulsan.ac.kr

Authors

Kwangsoo Kim − *Computational Science & Engineering Laboratory, Korea Institute of Energy Research, Daejeon 34129, Republic of Korea; Department of Chemical and Biomolecular Engineering, Yonsei University, Seoul 03722, Republic of Korea*; orcid.org/0000-0003-0395-2130

Jisoo Kim − *Clean Fuel Laboratory, Korea Institute of Energy Research, Daejeon 34129, Republic of Korea*

Kanghee Cho − *Clean Fuel Laboratory, Korea Institute of Energy Research, Daejeon 34129, Republic of Korea*; Present Address: Department of Chemistry and Chemical Engineering, Inha University, Inha-ro 100, Michuhol-gu, Incheon 22212, Republic of Korea; orcid.org/0000-0001-5942-4076

Sang-Sup Han − *Clean Fuel Laboratory, Korea Institute of Energy Research, Daejeon 34129, Republic of Korea*

Hyun Wook Kim − *Department of Chemical and Biological Engineering, Korea University, Seoul 02841, Republic of Korea*

Ki Bong Lee − *Department of Chemical and Biological Engineering, Korea University, Seoul 02841, Republic of Korea*; orcid.org/0000-0001-9020-8646

Byung-Hyun Kim − *Computational Science & Engineering Laboratory, Korea Institute of Energy Research, Daejeon 34129, Republic of Korea*; orcid.org/0000-0003-2493-5452

Jong Hyeok Park − *Department of Chemical and Biomolecular Engineering, Yonsei University, Seoul 03722, Republic of Korea*; orcid.org/0000-0002-6629-3147

Kyoungsoo Kim − *Department of Chemistry, Jeonbuk National University, Jeonju-si, Jeollabuk-do 54896, Republic of Korea*; orcid.org/0000-0002-2042-0913

Complete contact information is available at: https://pubs.acs.org/10.1021/acsami.3c04849

Author Contributions

‡C.H.L. and K.K. contributed equally.

Notes

The authors declare no competing financial interest.

ACKNOWLEDGMENTS

This work was conducted under the framework of the research and development program of National Research Foundation of Korea (NRF), funded by the Korean Government Ministry of Science and ICT (2022M3J2A1085669). C.H.L. acknowledges additional financial support by Regional Innovation Strategy (RIS) through the National Research Foundation of Korea (NRF) funded by the Ministry of Education (2021RIS-003).

REFERENCES

(1) Hao, G.-P.; Li, W.-C.; Qian, D.; Wang, G.-H.; Zhang, W.-P.; Zhang, T.; Wang, A.-Q.; Schüth, F.; Bongard, H.-J.; Lu, A.-H. Structurally Designed Synthesis of Mechanically Stable Poly(benzoxazine-co-resol)-Based Porous Carbon Monoliths and Their Application as High-Performance CO_2 Capture Sorbents. *J. Am. Chem. Soc.* **2011**, *133*, 11378−11388.

(2) Mo, Z.-W.; Zhou, H.-L.; Zhou, D.-D.; Lin, R.-B.; Liao, P.-Q.; He, C.-T.; Zhang, W.-X.; Chen, X.-M.; Zhang, J.-P. Mesoporous Metal-Organic Frameworks with Exceptionally High Working Capacities for Adsorption Heat Transformation. *Adv. Mater.* **2018**, *30*, 1704350.

(3) Fernández, J. A.; López, X.; Bo, C.; De Graaf, C.; Baerends, E. J.; Poblet, J. M. Polyoxometalates with Internal Cavities: Redox Activity, Basicity, and Cation Encapsulation in $[X^{n+}P_5W_{30}O_{110}]^{(15-n)-}$ Preyssler Complexes, with X = Na^+, Ca^{2+}, Y^{3+}, La^{3+}, Ce^{3+}, and Th^{4+}. *J. Am. Chem. Soc.* **2007**, *129*, 12244−12253.

(4) Das, S. K.; Wang, X.; Lai, Z. Facile Synthesis of Triazine-triphenylamine-Based Microporous Covalent Polymer Adsorbent for Flue Gas CO_2 Capture. *Microporous Mesoporous Mater.* **2018**, *255*, 76−83.

(5) Labrum, N. S.; Chen, C.-H.; Caulton, K. G. A bis-Pyrazolate Pincer on Reduced Cr Deoxygenates CO_2: Selective Capture of the Derived Oxide by Cr^{II}. *Chem.—Eur. J.* **2019**, *25*, 7935−7940.

(6) Kong, W.; Liu, Y.; Liu, J. Design of Highly Nitrogen-Doped, Two-Dimensional Hierarchical Porous Carbons with Superior Performance for Selective Capture of CO_2 and SO_2. *Energy Fuels* **2020**, *34*, 3557−3565.

(7) Wang, Y.; Hu, Z.; Kundu, T.; Cheng, Y.; Dong, J.; Qian, Y.; Zhai, L.; Zhao, D. Metal-Organic Frameworks with Reduced Hydrophilicity for Postcombustion CO_2 Capture from Wet Flue Gas. *ACS Sustainable Chem. Eng.* **2018**, *6*, 11904−11912.

(8) Huan, W.; Zhang, J.; Qin, H.; Huan, F.; Wang, B.; Wu, M.; Li, J. A Magnetic Nanofiber-Based Zwitterionic Hydrophilic Material for the Selective Capture and Identification of Glycopeptides. *Nanoscale* **2019**, *11*, 10952−10960.

(9) Lee, C. H.; Lee, K. B. Application of One-Body Hybrid Solid Pellets to Sorption-Enhanced Water Gas Shift Reaction for High-Purity Hydrogen Production. *Int. J. Hydrogen Energy* **2014**, *39*, 18128−18134.

(10) Lee, C. H.; Mun, S.; Lee, K. B. Application of Multisection Packing Concept to Sorption-Enhanced Steam Methane Reforming Reaction for High-Purity Hydrogen Production. *J. Power Sources* **2015**, *281*, 158−163.

(11) Lee, C. H.; Lee, K. B. Sorption-Enhanced Water Gas Shift Reaction for High-Purity Hydrogen Production: Application of a Na-Mg Double salt-Based Sorbent and the Divided Section Packing Concept. *Appl. Energy* **2017**, *205*, 316−322.

(12) Sarma, P. J.; Gardner, C. L.; Chugh, S.; Sharma, A.; Kjeang, E. Strategic Implementation of Pulsed Oxidation for Mitigation of CO Poisoning in Polymer Electrolyte Fuel Cells. *J. Power Sources* **2020**, *468*, 228352.

(13) Bang, G.; Moon, D.-K.; Kang, J.-H.; Han, Y.-J.; Kim, K.-M.; Lee, C.-H. High-Purity Hydrogen Production via a Water-Gas-Shift Reaction in a Palladium-Copper Catalytic Membrane Reactor Integrated with Pressure Swing Adsorption. *Chem. Eng. J.* **2021**, *411*, 128473.

(14) Sweatman, M. B.; Quirke, N.; Pullumbi, P. Predicting Ambient Temperature Adsorption of Gases in Active Carbons. *Stud. Surf. Sci. Catal.* **2007**, *160*, 95−103.

(15) Xue, C.; Hao, W.; Cheng, W.; Ma, J.; Li, R. Effect of Pore Size Distribution of Activated Carbon (AC) on CuCl Dispersion and CO Adsorption for CuCl/AC Adsorbent. *Chem. Eng. J.* **2019**, *375*, 122049.

(16) Tezel, F. H.; Apolonatos, G. Chromatographic Study of Adsorption for N_2, CO and CH_4 in Molecular Sieve Zeolites. *Gas Sep. Purif.* **1993**, *7*, 11−17.

(17) Yavary, M.; Ale Ebrahim, H.; Falamaki, C. Competitive Adsorption Equilibrium Isotherms of CO, CO_2, CH_4, and H_2 on Activated Carbon and Zeolite 5A for Hydrogen Purification. *J. Chem. Eng. Data* **2016**, *61*, 3420.

(18) Mishra, P.; Mekala, S.; Dreisbach, F.; Mandal, B.; Gumma, S. Adsorption of CO_2, CO, CH_4 and N_2 on a Zinc Based Metal Organic Framework. *Sep. Purif. Technol.* **2012**, *94*, 124.

(19) Bao, Z.; Chang, G.; Xing, H.; Krishna, R.; Ren, Q.; Chen, B. Potential of Microporous Metal-Organic Frameworks for Separation of Hydrocarbon Mixtures. *Energy Environ. Sci.* **2016**, *9*, 3612−3641.
(20) Bux, H.; Chmelik, C.; van Baten, J. M.; Krishna, R.; Caro, J. Novel MOF-Membrane for Molecular Sieving Predicted by IR-Diffusion Studies and Molecular Modeling. *Adv. Mater.* **2010**, *22*, 4741−4743.
(21) Yin, Y.; Wen, Z.; Shi, L.; Zhang, Z.; Yang, Z.; Xu, C.; Sun, H.; Wang, S.; Yuan, A. Cuprous/vanadium sites on MIL-101 for Selective CO Adsorption from Gas Mixtures with Superior Stability. *ACS Sustainable Chem. Eng.* **2019**, *7*, 11284−11292.
(22) Hirai, H.; Wada, K.; Kurima, K.; Komiyama, M. Carbon Monoxide Adsorbent Composed of Copper(I) Chloride and Polystyrene Resin Having Amino Groups. *Bull. Chem. Soc. Jpn.* **1986**, *59*, 2553−2558.
(23) Tamon, H.; Kitamura, K.; Okazaki, M. Adsorption of Carbon Monoxide on Activated Carbon Impregnated with Metal Halide. *AIChE J.* **1996**, *42*, 422−430.
(24) Huang, Y.; Tao, Y.; He, L.; Duan, Y.; Xiao, J.; Li, Z. Preparation of CuCl@AC with High CO Adsorption Capacity and Selectivity from CO/N_2 Binary Mixture. *Adsorption* **2015**, *21*, 373−381.
(25) Gao, F.; Wang, Y.; Wang, S. Selective Adsorption of CO on CuCl/Y Adsorbent Prepared using $CuCl_2$ as Precursor: Equilibrium and Thermodynamics. *Chem. Eng. J.* **2016**, *290*, 418.
(26) Kim, A.-R.; Yoon, T.-U.; Kim, S.-I.; Cho, K.; Han, S.-S.; Bae, Y.-S. Creating High CO/CO_2 Selectivity and Large CO Working Capacity through Facile Loading of Cu(I) Species into an Iron-Based Mesoporous Metal-Organic Framework. *Chem. Eng. J.* **2018**, *348*, 135−142.
(27) Chang, G.; Bao, Z.; Ren, Q.; Deng, S.; Zhang, Z.; Su, B.; Xing, H.; Yang, Y. Fabrication of Cuprous Nanoparticles in MIL-101: an Efficient Adsorbent for the Separation of Olefin-Paraffin Mixtures. *RSC Adv.* **2014**, *4*, 20230−20233.
(28) Zarca, G.; Ortiz, I.; Urtiaga, A. Copper(I)-Containing supported Ionic Liquid Membranes for Carbon Monoxide/Nitrogen Separation. *J. Membr. Sci.* **2013**, *438*, 38−45.
(29) Yoon, J. W.; Yoon, T.-U.; Kim, E.-J.; Kim, A.-R.; Jung, T.-S.; Han, S.-S.; Bae, Y.-S. Highly Selective Adsorption of CO over CO_2 in a Cu(I)-Chelated Porous Organic Polymer. *J. Hazard. Mater.* **2018**, *341*, 321−327.
(30) Kresse, G.; Hafner, J. Ab initio Molecular Dynamics for Liquid Metals. *Phys. Rev. B* **1993**, *47*, 558−561.
(31) Kresse, G.; Hafner, J. Ab initio Molecular-Dynamics Simulation of the Liquid-Metal-Amorphous-Semiconductor Transition in Germanium. *Phys. Rev. B* **1994**, *49*, 14251−14269.
(32) Kresse, G.; Furthmuller, J. Efficient Iterative Schemes for ab initio Total-Energy Calculations Using a Plane-Wave Basis Set. *Phys. Rev. B* **1996**, *54*, 11169−11186.
(33) Kresse, G.; Furthmuller, J. Efficiency of ab-initio Total Energy Calculations for Metals and Semiconductors Using a Plane-Wave Basis Set. *Comput. Mater. Sci.* **1996**, *6*, 15−50.
(34) Blöchl, P. E. Projector Augmented-Wave Method. *Phys. Rev. B* **1994**, *50*, 17953−17979.
(35) Kresse, G.; Joubert, D. From Ultrasoft Pseudopotentials to the Projector Augmented-Wave Method. *Phys. Rev. B* **1999**, *59*, 1758−1775.
(36) Perdew, J. P.; Burke, K.; Ernzerhof, M. Generalized Gradient Approximation Made Simple. *Phys. Rev. Lett.* **1996**, *77*, 3865−3868.
(37) Grimme, S.; Antony, J.; Ehrlich, S.; Krieg, H. A consistent and Accurate ab initio Parametrization of Density Functional Dispersion Correction (DFT-D) for the 94 Elements H-Pu. *J. Chem. Phys.* **2010**, *132*, 154104.
(38) Monkhorst, H. J.; Pack, J. D. Special Points for Brillouin-Zone Integrations. *Phys. Rev. B* **1976**, *13*, 5188−5192.
(39) Dudarev, S. L.; Botton, G. A.; Savrasov, S. Y.; Humphreys, C. J.; Sutton, A. P. Electron-Energy-Loss Spectra and the Structural Stability of Nickel Oxide: An LSDA+U study. *Phys. Rev. B* **1998**, *57*, 1505−1509.
(40) Teng, S. J.; Wang, J. N.; Xia, B. Y.; Wang, X. X. A General Strategy for the Preparation of Hollow Carbon Nanocages by NH_4Cl-Assisted Low-Temperature Heat Treatment. *Chem.—Eur. J.* **2010**, *16*, 13603−13608.
(41) Wang, J.-F.; Lin, L.; He, D.-N. Solid-State Synthesis of Nd-Doped Glass: Thermal Collapse of Nd^{3+}-Incorporated NaY Zeolites. *Inorg. Chem. Front.* **2017**, *4*, 183−190.
(42) Xu, J.; Mojet, B. L.; Lefferts, L. Effect of Zeolite Geometry for Propane Selective Oxidation on Cation Electrostatic Field of Ca^{2+} Exchanged Zeolites. *Microporous Mesoporous Mater.* **2006**, *91*, 187−195.
(43) Yang, Y.; Burke, N.; Zhang, J.; Huang, S.; Lim, S.; Zhu, Y. Influence of Charge Compensating Cations on Propane Adsorption in X Zeolites: Experimental Measurement and Mathematical Modeling. *RSC Adv.* **2014**, *4*, 7279−7287.
(44) Sen, D.; Kim, C. W.; Heo, N. H.; Seff, K. Using CuCl Vapor to Ion Exchange Copper Into Zeolite Na-Y. Single Crystal Structure of $|Cu_{30}Na_{30}Cl_9|[Si_{121}Al_{71}O_{384}]$-FAU Containing $Cu_{16}Cl_7^{21+}$, Cu_4Cl^{7+}, Cu_3Cl^{2+}, and Cu^{2+}. *Microporous Mesoporous Mater.* **2014**, *185*, 16−25.
(45) Li, Y.-X.; Ji, Y.-N.; Jin, M.-M.; Qi, S.-C.; Li, S.-S.; Xue, D.-M.; Yue, M.-B.; Liu, X.-Q.; Sun, L.-B. Controlled Construction of Cu(I) Sites within Confined Spaces via Host-Guest Redox: Highly Efficient Adsorbents for Selective CO Adsorption. *ACS Appl. Mater. Interfaces* **2018**, *10*, 40044−40053.
(46) Xie, Y.; Zhang, J.; Qiu, J.; Tong, X.; Fu, J.; Yang, G.; Yan, H.; Tang, Y. Zeolites Modified by CuCI for Separating CO from Gas Mixtures Containing CO_2. *Adsorption* **1997**, *3*, 27−32.
(47) Takahashi, A.; Yang, F. H.; Yang, R. T. Aromatics/Aliphatics Separation by Adsorption: New Sorbents for Selective Aromatics Adsorption by π-Complexation. *Ind. Eng. Chem. Res.* **2000**, *39*, 3856−3867.
(48) Yang, R. T. *Adsorbents : Fundamentals and Applications*; Wiley & Sons: Hoboken, NJ, 2003.
(49) Wang, Y.; Yang, R. T.; Heinzel, J. M. Desulfurization of Jet Fuel by π-Complexation Adsorption with Metal Halides Supported on MCM-41 and SBA-15 Mesoporous Materials. *Chem. Eng. Sci.* **2008**, *63*, 356−365.
(50) Bolis, V.; Maggiorini, S.; Meda, L.; D'Acapito, F.; Turnes Palomino, G.; Bordiga, S.; Lamberti, C. X-ray Photoelectron Spectroscopy and X-Ray Absorption Near Edge Structure Study of Copper Sites Hosted at the Internal Surface of ZSM-5 zeolite: A Comparision with Quantitative and Energetic Data on the CO and NH_3 Adsorption. *J. Chem. Phys.* **2000**, *113*, 9248−9261.
(51) Lamberti, C.; Turnes Palomino, G.; Bordiga, S.; Berlier, G.; D'Acapito, F.; Zecchina, A. Structure of Homoleptic $Cu^{I}(CO)_3$ Cations in Cu^{I}-Exchanged ZSM-5 Zeolite: An X-Ray Absorption study. *Angew. Chem., Int. Ed.* **2000**, *39*, 2138−2141.
(52) Yao, X.; Xiong, Y.; Zou, W.; Zhang, L.; Wu, S.; Dong, X.; Gao, F.; Deng, Y.; Tang, C.; Chen, Z.; Dong, L.; Chen, Y. Correlation Between the Physicochemical Properties and Catalytic Performances of $Ce_xSn_{1-x}O_2$ Mixed Oxides for NO Reduction by CO. *Appl. Catal., B* **2014**, *144*, 152−165.
(53) Bulánek, R. Investigation of IR vibrational band of C-O Bond of Carbonyl Species in Cu^{+}-MFI Zeolites. Phs. *Chem. Chem. Phys.* **2004**, *6*, 4208−4214.
(54) Hadjiivanov, K. I.; Kantcheva, M. M.; Klissurski, D. G. IR Study of CO Adsorption on Cu-ZSM-5 and CuO/SiO_2 Catalysts: σ and π Components of the Cu^{+}-CO Bond. *J. Chem. Soc. Faraday Trans.* **1996**, *92*, 4595−4600.
(55) Eswaramoorthi, I.; Sundaramurthy, V.; Dalai, A. K. Partial Oxidation of Methanol for Hydrogen Production over Carbon Nanotubes Supported Cu-Zn Catalysts. *Appl. Catal., A* **2006**, *313*, 22−32.
(56) Mehio, N.; Dai, S.; Jiang, D. E. Quantum Mechanical Basis for Kinetic Diameters of Small Gaseous Molecules. *J. Phys. Chem. A* **2014**, *118*, 1150−1154.
(57) Li, Q.; Shao, M.; Yu, G.; Wu, J.; Lia, F.; Qian, Y. A Solvent-Reduction Approach to Tetrapod-Like Copper(I) Chloride Crystallites. *J. Mater. Chem.* **2003**, *13*, 424−427.

https://doi.org/10.1021/acsami.3c04849
ACS Appl. Mater. Interfaces 2023, 15, 27411−27421

(58) Liu, S.; Hou, H.; Hu, W.; Liu, X.; Duana, J.; Meng, R. Binder-Free Integration of Insoluble Cubic CuCl Nanoparticles with a Homologous Cu Substrate for Lithium Ion Batteries. *RSC Adv.* **2016**, *6*, 3742−3747.
(59) Solomon, E. I.; Jones, P. M.; May, J. A. Electronic Structures of Active Sites on Metal Oxide Surfaces: Definition of the Copper-Zinc Oxide Methanol Synthesis Catalyst by Photoelectron Spectroscopy. *Chem. Rev.* **1993**, *93* (8), 2623−2644.

https://doi.org/10.1021/acsami.3c04849
ACS Appl. Mater. Interfaces 2023, 15, 27411−27421